Chapter 3

Experimental Details

In this chapter we describe experimental details, characteristics of the setups, the electron analyzers, and the soft X-ray beamlines employed. In addition, we summarize relevant aspects of sample preparation, experimental procedures, and applied PE geometries.

3.1 Sample preparation

Layer-resolved studies of the electronic and magnetic structure of crystal surfaces require samples of high structural and chemical quality. The case of rare-earth metals is especially demanding on the experimental conditions, due to their high chemical reactivity. Even in ultra-high vacua with residual pressures below 1×10^{-10} mbar, the electronic structure of a freshly prepared surface and its magnetic properties will be altered substantially within only several hours. Samples of bulk single crystals should be avoided; the problem of bulk impurity segregation to the surface makes the preparation of clean surfaces very difficult. High-quality lanthanide samples are rather prepared by epitaxial film growth on an appropriate substrate, typically a refractory-metal single crystal like tungsten.

The W(110) surface is particularly well suited as a substrate for the growth of monocrystalline lanthanide films for the following reasons:

- the (110) surface of a body-centered crystal is smooth on the atomic scale, giving small modulations of the substrate potential and activation energy for surface diffusion, therefore permitting high surface mobility of the adsorbed atoms;

- the high surface energy of the substrate lets one expect layer-by-layer or Stranski-Krastanov growth of the lanthanide metals on top of it;

- it matches rather well with the (0001) surface of the hcp lattice, causing only small lattice distortion;

- it is stable against formation of intermetallic compounds with most rare-earth metals. This allows one to anneal the films without the problem of alloy formation.

In addition, the comparatively fast cleaning procedure of the W(110) surface is also an important experimental advantage. The main contamination of a

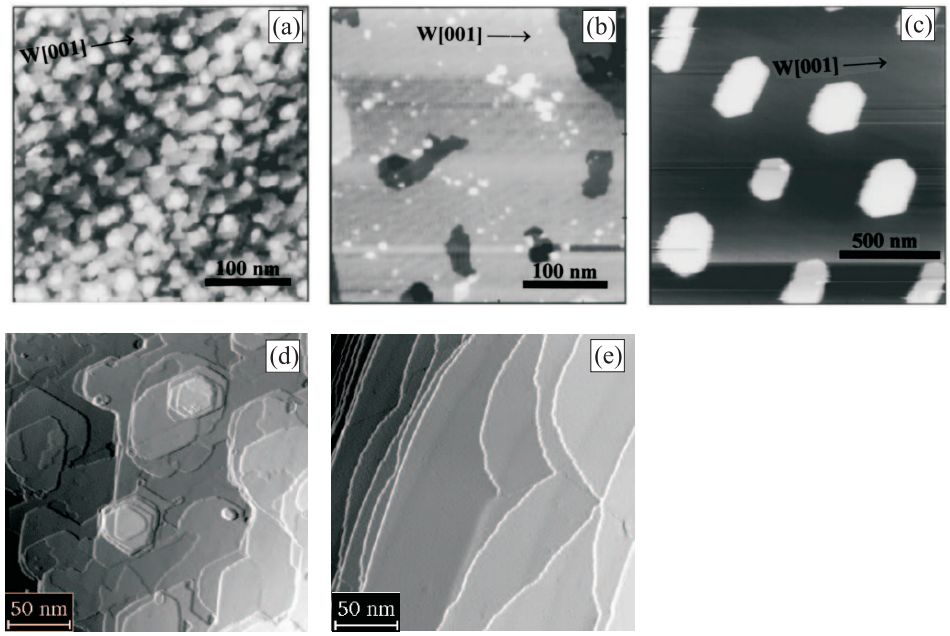

Figure 3.1: STM images illustrating different annealing steps of rare-earth metal film growth on a W(110) substrate. (a)-(c) 11-ML Gd(0001)/W(110) deposited at 300 K: (a) as deposited; (b) annealed at 530 K; (c) broken up into high islands (white) upon annealing at 710 K; from Ref. [26]. (d),(e) 10-nm Tb/W(110) film upon annealing at (d) 580 K, (e) 890 K.

bulk tungsten crystal is carbon. It can be removed by heating the crystal in oxygen atmosphere of 1×10^{-7} mbar at 1600 K. Under these conditions, carbon diffuses to the surface where it forms CO and CO_2 which desorbs from the surface at this temperature. Residual oxygen from this procedure can be removed by subsequent heating of the tungsten crystal for a few seconds to 2000 K. Also, the prepared rare-earth films can be removed by such a short "flash", i.e. no time-consuming sputtering/annealing cycles are needed here – maybe the greatest advantage of a tungsten substrate.

The quality of lanthanide films depends critically on the preparation conditions, in particular on evaporation rate, substrate temperature, and annealing temperature. The relation between growth parameters and film quality for lanthanides has been studied extensively during the past years with the result that standard procedures for evaporating each of the lanthanide elements from pure metal ingots are known.

The preparation of gadolinium single-crystalline films is performed by vacuum deposition at room temperature, followed by annealing at a temperature that depends on the film thickness [27]. For a 100-Å -thick film, annealing was performed at 660 K. For higher annealing temperatures, the film breaks up into islands [27]. This is illustrated in Fig. 3.1(a)-(c) for an 11-ML Gd film. Before annealing, the film is rough (3.1(a)), consisting of multiple-tiered structures and crevices. Annealing at 530 K results in a smooth film with only a few defects

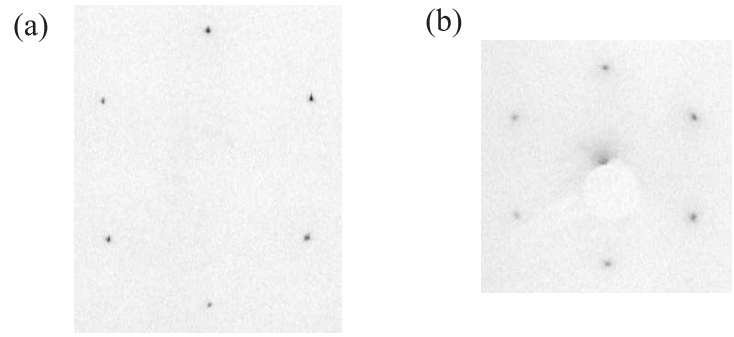

Figure 3.2: LEED patterns (inverted contrast) of (a) W(110) and (b) a 10-nm Gd(0001)/W(110) film, recorded at 100 eV and 80 K sample temperature.

(3.1(b)). If the film is annealed at 710 K, it is found to break up into islands that sit on top of a base monolayer of Gd (3.1(c)).

For terbium, the critical annealing temperature is higher. We have investigated the annealing behavior of Tb(0001) films on W(110) by STM in collaboration with M. Bode (Hamburg) [28]. We found that a 100-Å terbium film does not break up into islands upon annealing at 880 K (see Fig. 3.1(e)). Annealing at 580 K is not sufficient for Tb, leading to the formation of islands of rather small terrace width (Fig. 3.1(d)).

Alternatively, high-quality films can also be prepared by vacuum deposition at low substrate temperatures (20-80 K) with subsequent annealing. Sometimes this procedure can lead to an even higher quality of the prepared surface than deposition at room temperature adsorption (due to better vacuum conditions during evaporation); in the present work we used both preparation procedures, but no difference was observed in the results. We monitored the film quality *in situ* by low energy electron diffraction (near-surface crystal structure) and by angle-resolved photoemission (chemical cleanness).

Typical LEED results are presented in the Fig. 3.2: (a) sharp hexagonal pattern obtained from the W substrate and (b) from a Gd(0001) film; the latter indicates a well-ordered structure of the film.

Valence-band photoemission spectra corresponding to the Gd(0001) and Tb(0001) surfaces can be found in Chapter 10 (Fig. 10.1 for Gd and Fig. 10.15 for Tb). In angle-resolved photoemission, valence-band features and the 4f-line shape are closely related to the crystallinity of a film. Well-ordered films usually exhibit a pronounced valence-band dispersion, owing to electron emission from well-defined points in k-space (Brillouin zone). By contrast, valence-band spectra of purely ordered films rather show density-of-states intensity averaged over the Brillouin zone. The most distinctive feature of a smooth and chemically clean rare-earth surface is the sharp surface-state peak at the $\overline{\Gamma}$-point near the Fermi level (see inset in Fig. 10.1). In addition, one can judge the quality of a film from the energy separation between bulk and surface-shifted components of the 4f-line, owing to the high sensitivity of the core-level shift value to the atomic environment.

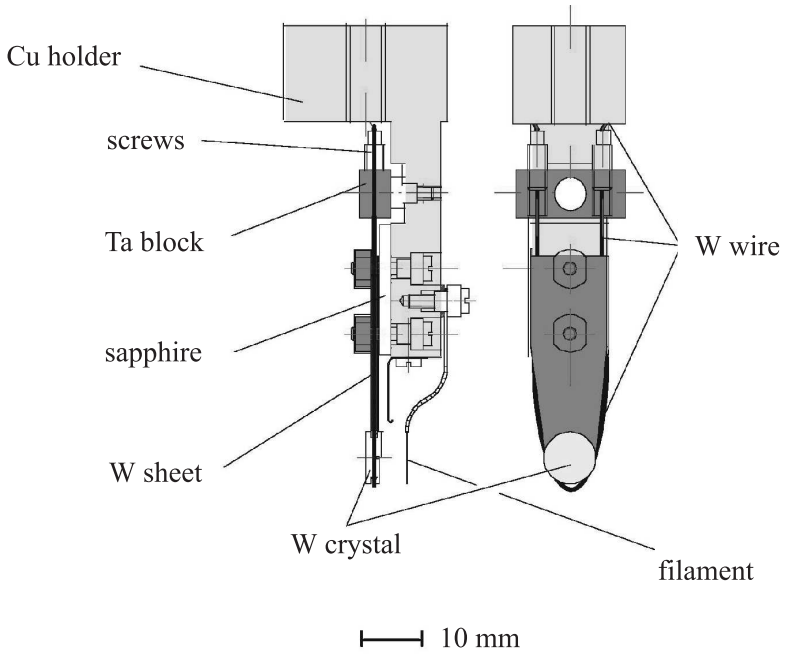

Figure 3.3: Schematics of the home-built sample holder that allows a temperature range of the W crystal between 20 K and 2000 K. The sapphire crystal provides electrical insulation together with good thermal contact at low temperatures.

Photoemission is significantly more sensitive to film impurities and surface contamination than LEED; typical surface contaminants like C, O, and even H can be monitored owing to their characteristic photoemission peaks in the valence-band region. Extremely high sensitivity for this can be achieved by choosing the proper photon energy.

Typically, it is possible to prepare practically contamination-free films (less than $\sim 1\%$ atomic concentration of C and O) after having achieved good vacuum conditions (low 10^{-11}-mbar range) and several cycles of film preparation.

3.2 Sample holder

Using a tungsten single crystal as substrate for rare-earth films and investigating of their magnetic properties by photoemission imposes several demands on the sample holder. These studies requires a particularly wide temperature range, including a careful temperature measurement. In addition, to prevent any remanent magnetic field near the sample, magnetic materials must be avoided in the vicinity of the sample holder.

The sample holder used in the present work is sketched in Fig. 3.3. The penny-shaped crystal has 8 mm diameter and is 3 mm thick. It is tied by a tungsten wire to a tungsten plate, which is fixed by a sapphire plate to the

coldfinger of a liquid-He flow cryostat. Fixed in this way, the crystal is electrically isolated from the cryostat. Single-crystalline sapphire has a good thermal conductivity at low temperatures, and it is a poor thermal conductor at higher temperatures. The construction in Fig. 3.3 permits to reach low temperatures down to 20 K, which is necessary for the present investigations. On the other hand, flashing the sample to 2000 K does not lead to a considerable temperature rise of the cryostat itself avoiding gas desorption from the environment of the sample holder. A tantalum filament is mounted behind the crystal (at $\sim$ 0.5 mm distance); it is wound in a such way ("bifilar") that magnetic field caused by the current through the filament is minimized. Crystal heating is achieved either by electron bombardment from the back of the crystal (for high temperatures) or by radiation heating through the heated filament (for lower temperatures).

For accurate temperature measurements it is important to have good thermal contact between the crystal and the sensor. A good (permanent) contact implies that the sensor should operate in the whole temperature range from 20 K to 2000 K. Only W-Re thermocouples are available for a such a wide temperature range. For this purpose, the W-Re thermocouple was squeezed between the wire and the crystal (cf. Fig. 3.3) to provide good thermal contact. The thermoelectric voltage of the W/Re thermocouple has an approximately parabolic temperature dependence with rather small differential thermopower at low temperatures ($\sim$ 20 K). To achieve maximum accuracy, the thermocouple wires were led uninterrupted from the sample to the precision millivoltmeter outside the chamber, by means of a home-built glued feed-through to avoid undefined contact voltages. The temperature accuracy with reference to 0° (ice water) was estimated to be better than 10 K below 100 K, and better than 3 K above 100 K.

After having assembled the crystal holder, it first had to pass a long degassing procedure in UHV (for several days) before PE experiments with clean films could be made. All parts of the cryostat serve as good absorbers for rest gas at low temperatures during the experiments, improving the vacuum conditions (base pressure is typically in the low 10^{-11}-mbar range), but a periodic warm-up of the cryostat in between experiments is recommended.

3.3 Evaporators

The rare-earth metal films investigated in this work were prepared by metal-vapor deposition from high-purity metals using home-build evaporators. To avoid alloying of the rare-earth metals, only high-purity refractory materials (tungsten and tantalum) were used in the evaporators. Fig. 3.4 shows a sketch of the typical construction. The evaporator consists of an electrically isolated tungsten crucible and a filament around it. To reduce heating of the chamber walls these central parts are surrounded by a shield of thin tantalum foil. All parts are fixed with tantalum rods on a standard feed-through flange. Standard cleaning procedures of the evaporators after construction were performed, followed by degassing in the UHV chamber at a temperature of 1600 K. Pieces

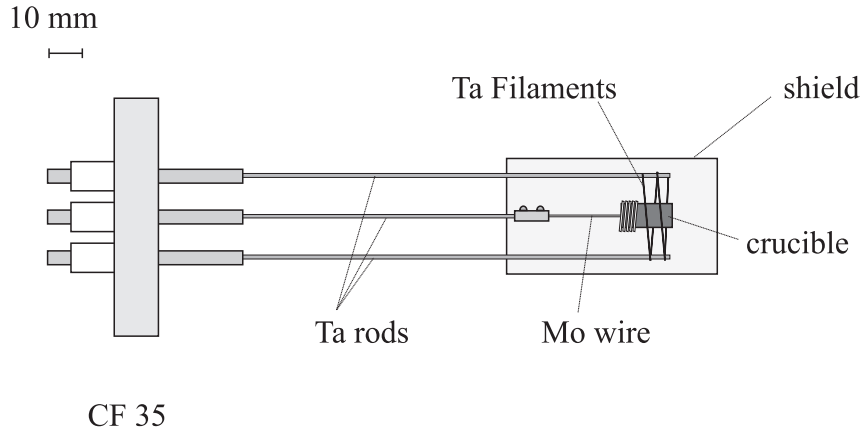

Figure 3.4: Home-built rare-earth metal evaporator mounted on a CF35 flange. Its relatively big size ensures high safety in operation (no risk of HV discharges). Uniform evaporation in a wide solid angle lowers the demand on the geometry of the substrate crystal installed in the vacuum chamber; in addition, these "open" evaporators serve as effective sublimation pumps.

of the rare-earth metal (99.99% purity) are put into the tungsten crucible and heated by electron bombardment, which permits to achieve a melting of most trivalent rare-earth metals. Just before filling of the evaporators, the metal ingots were mechanically scratched to remove surface contamination. Degassing of the evaporators in UHV and melting of the metals inside the crucible permitted to achieve pressures of $\sim 2 \times 10^{-10}$ mbar during evaporation, at a base pressure in the chamber of typically 3×10^{-11} mbar. The usual speed of evaporation was several angstroms per minute, as monitored by a quartz microbalance.

3.4 Magnet

Owing to the spatially integrating character of photoelectron spectroscopy its utilization in investigating the interplay between electronic and magnetic structures requires a single-domain state of the sample, with a well-defined magnetization direction. Moreover, PE experiments like magnetic dichroism, are typically performed with remanently magnetized samples without external magnetic fields, which would spoil the momentum resolution of the experiment. To magnetize the sample, one has to overcome the coercive field that can be substantial, particularly at low temperatures, where the magnetocrystalline anisotropy becomes large. These conditions define the requirements for the magnet to be used. On one side, it has to create a magnetic field in the kOe range, on the other side it should cause only small residual magnetic fields. In this work we used two types of magnets that are illustrated in Fig. 3.5.

The soft-iron cores are surrounded by about 1000 windings. To make the yoke magnetically soft, it was annealed for 36 h in hydrogen atmosphere at 1130 K, with subsequent slow cooling at a rate of about 30 K/h. This reduces

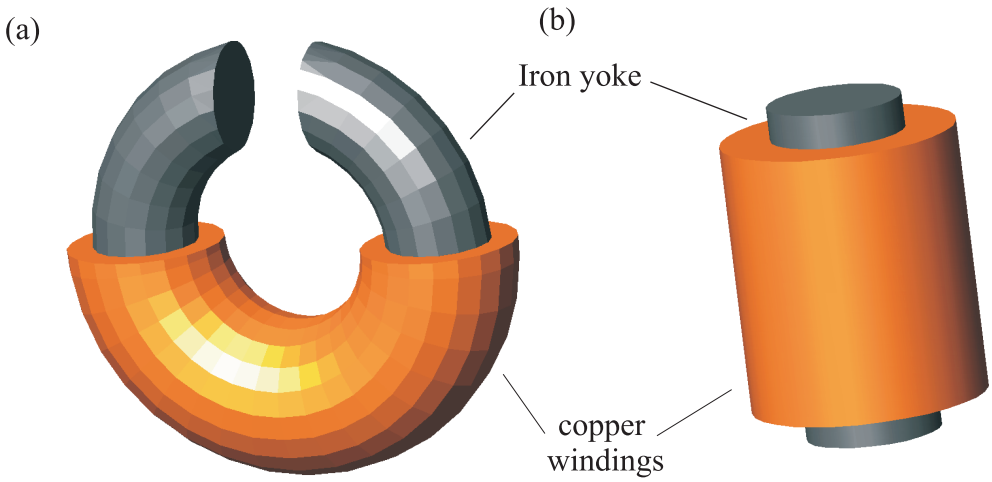

Figure 3.5: (a) Horseshoe-like type of iron yoke providing a strong and homogeneous magnetic field; (b) cylindrically-shaped magnet for pulse magnetization requiring a simpler setup geometry.

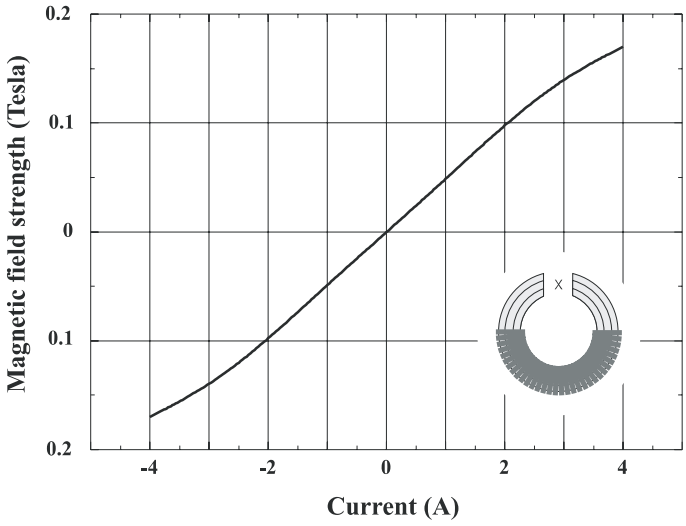

Figure 3.6: Calibration curve of the horseshoe iron-yoke magnet for mid-gap position, indicated by an x in the inset.

the concentration of impurities (typically S, C, N), which tend to make iron magnetically hard. The annealing procedure leads to a low residual remanent magnetic field of the yoke (below the earth field at the position of the sample) and it increases the maximum field strength by factor of two (compared to an unannealed yoke). The calibration curve of the yoke is shown in Fig. 3.6; the nonlinearity at high fields is due to saturation of the iron.

Finally, to avoid any influence of small residual fields of the magnet on the PE results we used an UHV-chamber array that consists of two separate chambers: sample preparation and magnetization were done in one chamber, while the photoemission analyzer was installed in a second chamber that is connected to the preparation chamber, but magnetically screened by a μ-metal shield at the inside walls.

3.5 Beamlines and endstations

The PE experiments were performed using linearly and circularly polarized radiation provided by undulator-based beamlines at the synchrotron radiation facilities BESSY II (Berlin, Germany) and MAX-lab (Lund, Sweden).

The U125/2 beamline at BESSY II has a spherical-grating monochromator and provides linearly-polarized light in the energy range from $\sim$ 35...400 eV. The experimental UHV system consists of a preparation chamber and a PE chamber with a hemispherical electron energy analyzer (SCIENTA SES 100). The analyzer can be rotated by $\pm 8^\circ$ around the initial angle between the analyzer and the incoming light, which is 60°.

For the experiments with circularly polarized soft X-ray radiation the beamline U56/2 PGM2 was utilized (energy range: 90...1300 eV). The degree of circular polarization was higher than 95% at the energies used in the experiments.

Some experiments in this dissertation were performed at the I311 beamline of the Swedish synchrotron radiation source (MAX-lab). It is an undulator-based, soft X-ray beamline dedicated to high-resolution X-ray photoelectron spectroscopy (XPS) and X-ray absorption spectroscopy (XAS) on clean and adsorbate-covered surfaces. Like at the U125/2 beamline at BESSY, the endstation consists of separate analyzer and preparation chambers. It is equipped with a hemispherical electron energy analyzer (SCIENTA SES 200) mounted at an angle of 55° with respect to the incoming light direction (energy range: 30...1500 eV, photon flux at the sample position: 10^{11} - 10^{13} photons/s).

3.6 Experimental geometries

Figures 3.7 and 3.8 represent the two experimental geometries, which we used in case of circularly and linearly polarized light excitation, respectively. In both cases, the sample was magnetized in the sample-surface plane.

In magnetic circular dichroism experiments, the magnetization direction was parallel to the plane defined by the incoming light propagation direction and the electron-emission direction (scattering plane) as sketched in Fig. 3.7. The smallest possible angle $\theta^{h\nu} = 15^\circ$ was used to achieve practically pure $\Delta M = +1$

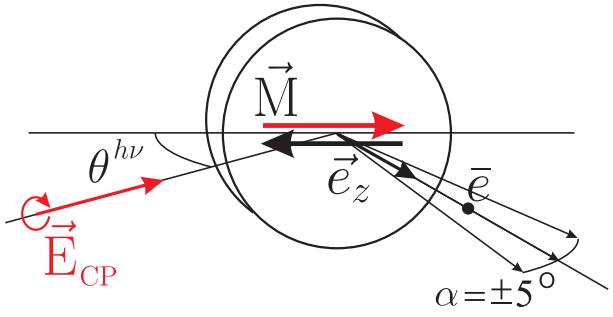

Figure 3.7: Geometry used in the experiments with circularly polarized light.

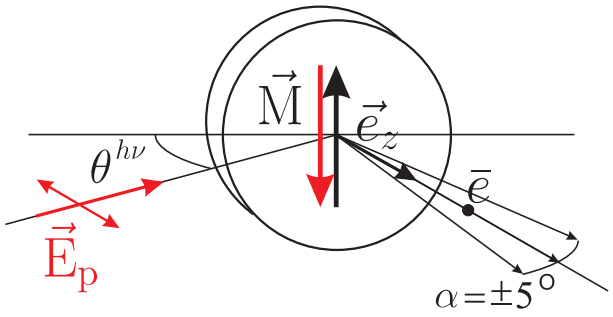

Figure 3.8: Geometry used in the experiments with linearly polarized light.

or $\Delta M = -1$ transitions (see section 4.4) upon magnetization reversal (red and black arrows). The electron emission at near-surface-normal angles was studied.

In the experiments with linearly polarized light (magnetic linear dichroism and Rashba effect), the samples were magnetized perpendicular to the scattering plane (Fig. 3.8), according to the considerations in Chapter 4; this leads to maximum values of the dichroic signal as well as limiting cases for the Rashba effect for the two opposite magnetizations (red and black arrows). The angle $\theta^{h\nu} = 35°$ (or 30°) was defined in this case by the fixed position of the analyzer with respect to the incoming-light direction. These angles are close to the one at which the atomic dichroism effect has its the maximum value ($\theta^{h\nu} = 45°$), but this is not important for the Rashba effect. For diffraction effects this is an important parameter that will be specified in each particular case. Electron-emission angles near surface normal were employed.